Molecular and Cellular Neuroscience 50 (2012) 147–159

Contents lists available at SciVerse ScienceDirect

Molecular and Cellular Neuroscience

journal homepage: www.elsevier.com/locate/ymcne

Long term potentiation affects intracellular metalloproteinases activity in the mossy fiber — CA3 pathway

Grzegorz Wiera [a,b,*], Tomasz Wójtowicz [a], Katarzyna Lebida [a], Aleksandra Piotrowska [c], Dominika Drulis-Fajdasz [a,b], Agnieszka Gomułkiewicz [c], Daria Gendosz [a], Marzena Podhorska-Okołów [c], Marco Capogna [d], Grzegorz Wilczyński [e], Piotr Dzięgiel [c], Leszek Kaczmarek [f], Jerzy W. Mozrzymas [a,b,*]

[a] Laboratory of Neuroscience, Department of Biophysics, Wroclaw Medical University, Chalubinskiego 3, 50-368, Wroclaw, Poland
[b] Department of Animal Molecular Physiology, Zoological Institute, Wroclaw University, Cybulskiego 30, 50-205, Wroclaw, Poland
[c] Department of Histology and Embryology, Wroclaw Medical University, Chalubinskiego 6A, 50-368, Wroclaw, Poland
[d] Anatomical Neuropharmacology Unit, Medical Research Council, Mansfield Road, Oxford OX1 3TH, United Kingdom
[e] Laboratory of Molecular and Systemic Neuromorphology, Nencki Institute, Ludwika Pasteura 3, 02-093, Warsaw, Poland
[f] Department of Molecular and Cellular Neurobiology, Nencki Institute, Ludwika Pasteura 3, 02-093, Warsaw, Poland

ARTICLE INFO

Article history:
Received 7 October 2011
Revised 6 April 2012
Accepted 13 April 2012
Available online 25 April 2012

Keywords:
LTP
Metalloproteinase
Mossy fiber
Hippocampus
Synaptic plasticity
MMP-9

ABSTRACT

Matrix Metalloproteinases (MMPs) are a family of endopeptidases known to process extracellular proteins. In the last decade, studies carried out mainly on the Schaffer collateral — CA1 hippocampal projection have provided solid evidence that MMPs regulate synaptic plasticity and learning. Recently, our group has shown that MMP blockade disrupts LTP maintenance also in the mossy fiber-CA3 (mf-CA3) projection (Wojtowicz and Mozrzymas, 2010), where LTP mechanisms are profoundly different (NMDAR-independent and presynaptic expression site). However, how plasticity of this pathway correlates with activity and expression of MMPs remains unknown. Interestingly, several potential MMP substrates (especially of gelatinases) are localized intracellularly but little is known about MMP activity in this compartment. In the present study we have asked whether LTP is associated with the expression and activity of gelatinases in apparent intra- and extracellular compartments along mf-CA3 projection. *In situ* zymography showed that LTP induction was associated with increased gelatinases activity in the cytoplasm of the hilar and CA3 neurons. Using gelatin zymography, immunohistochemistry and immunofluorescent staining we found that this effect was due to *de novo* synthesis and activation of MMP-9 which, 2–3 h after LTP induction was particularly evident in the cytoplasm. In contrast, MMP-2 was localized preferentially in the nuclei and was not affected by LTP induction. In conclusion, we demonstrate that LTP induction in the mf-CA3 pathway correlates with increased expression and activity of MMP-9 and provide the first evidence that this increase is particularly evident in the neuronal cytoplasm and nucleus.

Introduction

Matrix Metalloproteinases (MMPs) are a family of endopeptidases commonly implicated in degradation, turnover and processing of extracellular matrix (ECM) and pericellular proteins (Butler and Overall, 2009; Cauwe and Opdenakker, 2010; Cauwe et al., 2007). It is known that these enzymes play a crucial role in egg fertilization, embryonic development, wound healing, apoptosis, metastasis and inflammatory processes. In the last decade, MMPs have also been discovered as fine regulators of physiological and pathological functions of neurons and neuronal networks (Ethell and Ethell, 2007; Rivera et al., 2010; Szklarczyk and Conant, 2010; Wlodarczyk et al., 2011; Yong, 2005). More specifically, MMPs were found to play an important role in learning and synaptic plasticity phenomena. In particular, MMP inhibition prevented the hippocampus-dependent learning and impaired the maintenance of long term potentiation (LTP) in the Schaffer

Abbreviations: APMA, 4-aminophenyl mercuric acid; CHX, cycloheximide; fEPSP, field excitatory postsynaptic potential; GFAP, glial fibrillary acidic protein; ISZ, *in situ* zymography; LTP, long term potentiation; mf-CA3, mossy fiber-CA3; MAP-2, microtubule associated protein 2; MMP, matrix metalloproteinase; PARP-1, poly-ADP-ribose polymerase-1; PMSF, phenylmethylsulfonyl fluoride; ROI, region of interest; TIMP, tissue inhibitor of matrix metalloproteinase.

* Corresponding authors at: Laboratory of Neuroscience, Department of Biophysics, Wroclaw Medical University, Chalubinskiego 3, 50-368 Wroclaw, Poland. Fax: +48 71 784 1399.

E-mail addresses: gwiera@biol.uni.wroc.pl (G. Wiera), tomasz.wojtowicz@am.wroc.pl (T. Wójtowicz), sucha5@interia.pl (K. Lebida), ola@hist.am.wroc.pl (A. Piotrowska), drulis.fajdasz@biol.uni.wroc.pl (D. Drulis-Fajdasz), agom@hist.am.wroc.pl (A. Gomułkiewicz), mapod@hist.am.wroc.pl (M. Podhorska-Okołów), marco.capogna@pharm.ox.ac.uk (M. Capogna), g.wilczynski@nencki.gov.pl (G. Wilczyński), piotr@hist.am.wroc.pl (P. Dzięgiel), l.kaczmarek@nencki.gov.pl (L. Kaczmarek), jerzy.mozrzymas@am.wroc.pl (J.W. Mozrzymas).

1044-7431/$ – see front matter © 2012 Elsevier Inc. All rights reserved.
doi:10.1016/j.mcn.2012.04.005

collaterals — CA1 (Sch-CA1) synapses (Meighan et al., 2006, 2007; Nagy et al., 2006; Wang et al., 2008). Noteworthy, among MMPs, a gelatinase MMP-9 appears to be particularly strongly involved in learning and synaptic plasticity *in vitro* (Meighan et al., 2006, 2007; Nagy et al., 2006; Wang et al., 2008) and *in vivo* (Bozdagi et al., 2007; Okulski et al., 2007; Spolidoro et al., 2012). Moreover, increased level of MMP-9 was found to correlate with plasticity induction and learning (Meighan et al., 2006; Nagy et al., 2006; Wright et al., 2006).

Most evidence concerning involvement of MMPs in synaptic plasticity and hippocampus-dependent learning came from studies on the Sch-CA1 projection, where the LTP induction and its expression sites are believed to be postsynaptic. Recently, we have shown that pharmacological blockade of MMPs disrupts the maintenance of LTP in the mossy fiber — CA3 hippocampal (mf-CA3) projection where LTP is independent of NMDA receptors and its expression site is presynaptic (Nicoll and Schmitz, 2005; Wojtowicz and Mozrzymas, 2010). This result suggests a universal role of MMPs in the consolidation of synaptic plasticity phenomena controlled by profoundly different mechanisms. In spite of growing body of evidence about a crucial role of MMPs in learning and synaptic plasticity, little is known about the underlying molecular mechanisms. In particular, whether or not induction of plasticity phenomena in mf-CA3 pathway is correlated with changes in MMPs expression and activity remains unknown. In the past decade, biochemical, proteomic and degradomic techniques have greatly extended the substrate repertoire of the MMPs (Cauwe and Opdenakker, 2010; Overall, 2002). Importantly, as correctly pointed out by Cauwe and Opdenakker (2010), a substantial part of putative substrates of MMPs is localized intracellularly (nucleus, mitochondria, various vesicles and cytoplasm, often in association with cytoskeleton) making thus the classical view of MMPs as enzymes operating solely in extracellular space no longer adequate. It needs to be emphasized that the largest number of putative intracellular substrates has been indicated for gelatinases (MMP-2 or MMP-9, see Table 3 in Cauwe and Opdenakker, 2010) and many of them are functionally coupled with processes of synaptic plasticity such as glycogen synthase kinase-3β, myosin heavy chain, α-synuclein or poly(ADP-ribose) polymerase (Butler and Overall, 2009). These data suggest thus a potentially prominent role of gelatinases in the intracellular signaling and it is likely that phenomena of synaptic plasticity might depend, at least in part, on their intraneuronal activity. However, so far, intracellular MMPs have not been systematically investigated in the context of physiological processes such as synaptic plasticity. Taking into account a crucial role of MMPs in maintenance of LTP in the mf-CA3 pathway (Wojtowicz and Mozrzymas, 2010), we have extended this issue by asking whether LTP in this projection is associated with alterations in the expression and activity of gelatinases in apparent intra- and extracellular neuronal compartments. By using *in situ* and gel zymography, immunohistochemistry as well as pharmacological and electrophysiological tools, we provide the first evidence that LTP induction in mf-CA3 pathway gives rise to increased gelatinases activity in neuronal soma (predominantly MMP-9) and to a smaller extent in its surroundings which is likely to include glia, neuronal processes and extracellular milieu.

Results

LTP is associated with increased DQ-gelatin fluorescence in CA3 and hilus

To address the involvement of gelatinases in the plasticity of mf-CA3 pathway, we performed *in situ* zymography on hippocampal slices collected and fixed immediately after electrophysiological recordings (i.e. approximately 2 h after LTP induction for LTP group or 2–3 h of basal stimulation for control group). In this technique, the fluorogenic substrate DQ-gelatin becomes a source of fluorescence when cleaved by gelatinases (Fig. 1A). First, we analyzed the total DQ fluorescence in CA3 region of 4 μm thin sections of hippocampal slices with wide-field fluorescence microscope (see Experimental methods for details). On average, the total DQ fluorescence in CA3 increased by 30% in LTP slices relative to control slices (average values were 753.0 ± 48.5 and 575.6 ± 34.2 arbitrary units [AU], for LTP and control slices, respectively, $n = 8$ and 6 slices, $p < 0.01$).

To further explore the difference between DQ fluorescence in the control and LTP groups, we performed a detailed analysis for three different areas in the CA3 region: apparent extracellular space, nuclei and cytoplasm. To distinguish neurons from other cell types, DQ-gelatin treated sections were additionally stained against MAP-2. Importantly, this staining enabled us to precisely define the limits of neuronal bodies and proximal dendrites (Fig. 1A). The analysis of respective areas was carried out within regions of interest (ROIs) manually drawn or depicted by means of computer- and visually-guided threshold algorithm (see Experimental methods).

Since gelatinases can be released from neurons or astrocytes, it is interesting to analyze the DQ fluorescence in apparent extracellular space in the CA3 region. For this purpose, we selected appropriate area with the threshold method based on visual inspection and MAP-2 staining and calculated weighted average of fluorescence (see Experimental methods, Fig. 1B). As presented in Fig. 1C, average DQ fluorescence in apparent extracellular space increased by nearly 26% in slices collected 2 h post LTP relative to control slices (522.3 ± 37.0 and 415.8 ± 30.2 AU, respectively, $n = 8$–10 slices per group, $p < 0.05$). This increase was further illustrated by a shift in the cumulative histogram constructed for mean values of apparent extracellular fluorescence in all collected images in respective groups ($n = 98$ and 126 images for LTP and control slices, respectively, K-S statistics = 0.37, $p < 0.001$, Fig. 1D).

DQ fluorescence was particularly intense in neuronal nuclei (Fig. 1A). However, the mean nuclei-associated DQ fluorescence did not significantly differ between LTP and control slices (1702.8 ± 170.4 and 1718.5 ± 124.1 AU, for MAP-2 positive neurons in LTP and control slices respectively, $n = 5$ and 7 slices, $p = 0.94$, Fig. 1F). This result is further confirmed by the lack of any significant shift in the cumulative histograms when all analyzed nuclei are considered ($n = 636$ and 1297 nuclei in control and LTP group, respectively, K-S statistics = 0.069, $p > 0.05$, Fig. 1G).

Interestingly, *in situ* zymography revealed that cytoplasm-associated DQ fluorescence was markedly stronger than in the cells' surroundings (see confocal images in Fig. 1A). Moreover, for the cells in which MAP-2 staining was continuous, a clear overlap of MAP-2 with increased DQ-gelatin fluorescence signal was seen (Fig. 1A). We thus made an attempt to assess the DQ fluorescence in the cytoplasmic MAP-2 positive localizations in the CA3 region. However, a strong DQ fluorescence associated with neuronal nuclei gave rise to scattered light in non-focal planes (i.e. glow) that partially overlapped with signal from the cytoplasm making the quantification of fluorescence in this compartment unreliable. For this reason, we applied laser scanning confocal microscopy and acquired a series of high resolution images (see Experimental methods for details). The analysis was performed in sum-projected stacks on a subset of neurons characterized with continuous MAP-2 staining of soma and proximal apical dendrite. An important issue in this analysis was a marked cell-to-cell variability of the cytoplasm fluorescence as well as of background fluorescence between sections. To reduce the variability due to these factors, for each image the measured intracellular fluorescence was normalized to average extracellular fluorescence and expressed as F_{int}/F_{ext} ratio (Fig. 1I, see Experimental methods for details). It should be emphasized that although this procedure reduced the data scatter, it underestimated the difference between control and LTP group because in the CA3 region, as described above, LTP induction led to the upregulation of the apparent extracellular signal by approximately 26% (Fig. 1C). As shown in Fig. 1J, in the CA3 region, the average F_{int}/F_{ext} ratios were significantly larger in LTP slices than in the respective

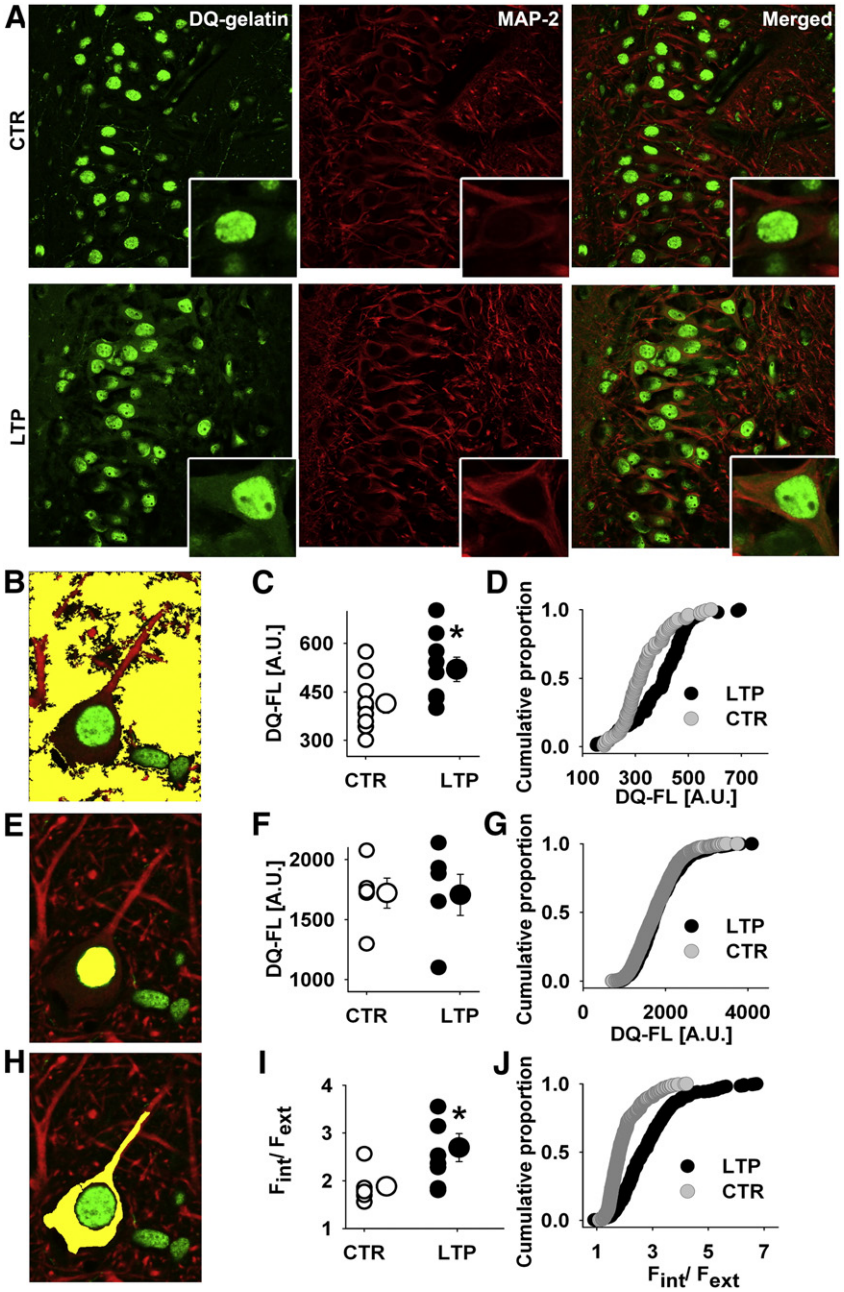

Fig. 1. LTP in mf-CA3 is associated with changes in DQ-gelatin fluorescence in CA3 region. A, Representative images of CA3 region of control hippocampal slice (top row) and 2 h post LTP induction in mf-CA3 pathway (bottom row). Sections were incubated with DQ-gelatin and counterstained with MAP-2, a neuronal marker. Note a difference in DQ fluorescence intensities between control and LTP slices. Insets show soma of individual CA3 pyramidal neuron from the same section. Note increase in cytoplasmic DQ fluorescence post LTP. B, Pictorial image showing the apparent extracellular space (yellow area) determined with the threshold method (see Experimental methods for details). C, Statistics of DQ fluorescence in apparent extracellular space. Small circles represent the average values obtained for single slices (n = at least 8 slices). Large circles indicate the mean values for controls and LTP groups (open and filled circles represent control and LTP groups, respectively). Asterisk indicates statistical significance ($p<0.05$, unpaired t-test). D, Cumulative histogram of mean fluorescence intensity in apparent extracellular space in all images inspected in this study. Note a shift of fluorescence associated with LTP. E, Pictorial image showing the nuclei manually encircled for further analysis of DQ fluorescence (yellow circle). F, Statistics of DQ fluorescence in nuclei of CA3 *stratum pyramidale* neurons (n = at least 5 slices). Legend as in C. G, Cumulative histogram of fluorescence intensity in the nuclear area of CA3 *stratum pyramidale* neurons in all images inspected in this study. Note that the distribution of mean fluorescence in nuclei in LTP slices does not differ from that in control slices. H, Pictorial image showing the encircled neuronal cytoplasm (yellow) where fluorescence (F_{int}) was analyzed. I, Statistics of F_{int}/F_{ext} values for CA3 *stratum pyramidale* neurons (n = at least 6 slices). Legend as in C. J, Cumulative histogram of intracellular to apparent extracellular fluorescence ratio (F_{int}/F_{ext}) analyzed in CA3 *stratum pyramidale* neurons in all images inspected in this study. Note that the distribution of (F_{int}/F_{ext}) in LTP slices is significantly shifted towards higher values with respect to control slices.

controls (average F_{int}/F_{ext} ratios were 2.68 ± 0.29 and 1.86 ± 0.15, $n = 8$ and 6 slices, respectively, $p<0.05$, Fig. 1I). This finding is additionally visualized by a clear shift in the cumulative histogram of F_{int}/F_{ext} ratios of all CA3 (MAP-2 positive) neurons from LTP slices with respect to control slices ($n = 364$ and 432 neurons, respectively, K-S statistics = 0.48, $p<0.001$, Fig. 1J).

Since mossy fibers, on their way to CA3 region innervate various excitatory and inhibitory neurons in the hilus (Acsady et al., 1998), analogous analysis of DQ fluorescence was performed for MAP-2 positive neurons in the hilar region. We found that fluorescence associated with apparent extracellular space in LTP slices increased by 19% relative to control slices but this change, at variance to the CA3 region,

did not reach statistical significance (average values were 538.9 ± 55.9 and 449.6 ± 32.8 AU for LTP and control slices, respectively, $n = 7$ and 8 slices in each group, $p = 0.17$, Supplemental Fig. S2). Similar to CA3 region, the mean fluorescence intensity associated with nuclei (analyzed in the wide-field fluorescence mode) was not different between LTP and control slices (average values were 1834.7 ± 396.2 and 2042.2 ± 354.5 AU for LTP and control slices, respectively, $n = 3$ and 4 slices in each group, $p = 0.7$, Fig. 1). Mean average MAP-2 staining intensity did not show any significant difference between LTP and control group (785 ± 11 and 792 ± 12 AU, $n = 5$ and $n = 7$ for control and LTP slices respectively, $p > 0.05$). Altogether, these results indicate that LTP in mf-CA3 pathway is accompanied by a marked upregulation of gelatinolytic activity.

MMP-2 and MMP-9 are the main source of the cytoplasmic and extracellular DQ-gelatin fluorescence

To identify proteases, contributing to DQ-gelatin digestion, different protease inhibitors were tested by applying them throughout the entire process of *in situ* zymography (slice hydratation, reaction with DQ-gelatin and washing). PMSF (0.2–1 mM) a serine protease inhibitor, had no effect on the mean DQ-gelatin fluorescence in the dentate gyrus, and CA3 region (for CA3 *stratum pyramidale* weighted mean DQ-gelatin florescence was 107 ± 24% in the presence of 0.2 mM PMSF relative to control group, $n = 3$ slices in PMFS and 5 slices in control group; $p = 0.86$; Fig. 2A,B). However, the MMP pan-inhibitor phenanthroline (10 mM), a potent zinc chelator that inhibits all MMPs and GM-6001 (1 mM) largely abolished the DQ-gelatin fluorescence (Fig. 2A, B), consistent with a previous study by Gawlak et al. (2009). Another MMP inhibitor FN-439, which besides blocking MMP-1,-3,-8 shows a relatively high potency for gelatinases (Ic50 *in vitro* 30 μM for MMP-9 and <25 μM for MMP-2, Franzke et al., 2002; Odake et al., 1994), reduced the mean DQ-gelatin fluorescence in CA3 stratum pyramidale by more than one half relative to non-treated slices (42 ± 9% of mean DQ-gelatin fluorescence in the presence of 1–5 mM FN-439 $n = 4$, relative to group without inhibitor where $n = 5$, all sections came from LTP group, $p < 0.01$ Fig. 2B,C). It indicates that most of observed gelatinolytic activity could be attributed to gelatinases. Importantly, the remaining DQ-gelatin fluorescence was almost exclusively found in nuclei and no detectable signal was present either in the cytoplasm of CA3 neurons or in the apparent extracellular space (Fig. 2C). Since the fluorescence intensity quantified in sections incubated without DQ-gelatin was negligible, we conclude that gelatinases (MMP-2 and MMP-9) are the main source of the cytoplasmic and extracellular DQ-gelatin fluorescence in our model.

LTP induction in mf-CA3 pathway leads to upregulation of active and latent MMP-9 forms

Results obtained using *in situ* zymography indicate an upregulation of gelatinases' activity. However, the relative contributions of MMP-2 and MMP-9 to these changes remain unknown. Moreover, it needs to be taken into consideration that the latent form of these MMPs might contribute to some extent to the DQ-gelatin fluorescence (Bannikov et al., 2002). We therefore have made an attempt to establish to what extent LTP in mf-CA3 pathway affected the active and latent MMP-9 pools. To this end, we used gelatin substrate gel zymography which offers an advantage with respect to the *in situ* zymography in that it distinguishes inactive and active gelatinases. Thus, we reasoned that a precise assessment of active and latent MMP-9 forms in the gel zymogram should provide us with a reliable, although indirect, clue about the expression of these MMP-9 forms. For this purpose, we have compared the bands corresponding to the active and latent gelatinases in extracts from control and LTP slices containing the dentate gyrus and CA3 region. Our extraction procedure gave final

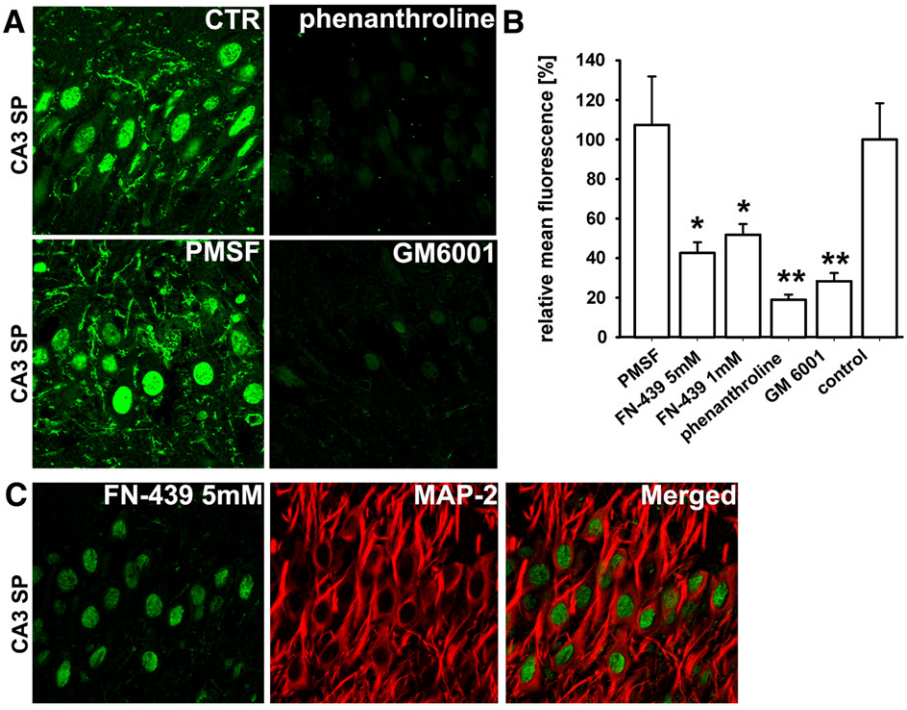

Fig. 2. Phenanthroline, GM6001 and more specific gelatinase inhibitor FN-439 block the DQ-gelatin fluorescence in contrast to the serine proteases inhibitor — PMSF. A, Representative confocal images show *in situ* zymography in CA3 *stratum pyramidale* (CA3 SP) conducted in presence of protease inhibitors: phenanthroline 10 mM, GM6001 1 mM, and PMSF 0.2 mM during hydratation, enzymatic reaction, and washouts steps relative to control. Note unchanged gelatinolytic activity pattern in presence of serine proteases inhibitor PMSF. B, Mean DQ fluorescence signal in CA3 stratum pyramidale in presence of 0.2 mM PMSF ($n = 4$), 1 and 5 mM FN-439 (both $n = 2$), 10 mM phenanthroline ($n = 4$), 1 mM GM6001 ($n = 4$) relative to reaction without inhibitors ($n = 6$). All sections used in these experiments were from the LTP group. C, Representative ISZ showing gelatinase activity in the CA3 stratum pyramidale in LTP group in the presence of FN-439 (5 mM) counterstained with MAP-2 (red). Note the lack of DQ-gelatin fluorescence in neuronal cytoplasm, and diminished signal in nuclei.

samples enriched in ECM, cytoskeleton and membrane bound proteins (see for details Experimental methods). Zymograms of tissue extracts showed two bands of MMP-9 gelatinolytic activity (proMMP-9 at 95–100 kDa and active or intermediate form MMP-9 at 88–90 kDa) (Zhang and Gottschall, 1997). Densitometric analysis of zymograms revealed that respective bands corresponding to pro and active MMP-9 forms were upregulated within 2–3 h after LTP induction in mf–CA3 pathway (proMMP-9 increased by 87 ± 30% and active MMP-9 by 54 ± 14%; respectively, $p<0.05$, $n=4$ experiments, Fig. 3A). Since gel zymography for control and LTP groups was performed under exactly the same conditions and both bands (for active and latent MMP-9) were significantly increased, these data provide a clear, although indirect indication that LTP induction caused an increase in expression of MMP-9 in the considered pathway.

To provide further support for this observation, we have checked whether LTP-induced MMP-9 increase depends on *de novo* protein synthesis in the mf-CA3 pathway. For this purpose, we have investigated the impact of LTP induction on MMP-9 in slices incubated with protein synthesis inhibitor cycloheximide (CHX, 60 μM). Cycloheximide had no effect on basal synaptic transmission of mf-CA3 pathway (data not shown), similar to what previously reported by Calixto et al. (2003). In addition, short-term plasticity protocols (paired pulse, burst facilitation) applied before and 2 h after LTP induction did not reveal any significant difference between control and CHX-treated slices. However, protein synthesis inhibitor clearly abolished fEPSP potentiation as early as 30 min after LTP induction (187 ± 14% and 117 ± 7%, in control and CHX-treated slices, respectively, $n=3$ and 4, $p<0.05$; Fig. 3C) as previously shown (Calixto et al., 2003). Gelatin zymography performed on tissue extracts from CHX-treated slices showed that the LTP-induced increase in the intensity of bands corresponding to MMP-9 latent and active forms was abolished with a trend to a reduction probably due to ongoing protein degradation ($p>0.05$, Fig. 3B). Altogether, these results suggest that LTP in mossy fiber pathway is associated with increased activity and expression of MMP-9 and point to a crucial role of protein synthesis is these processes.

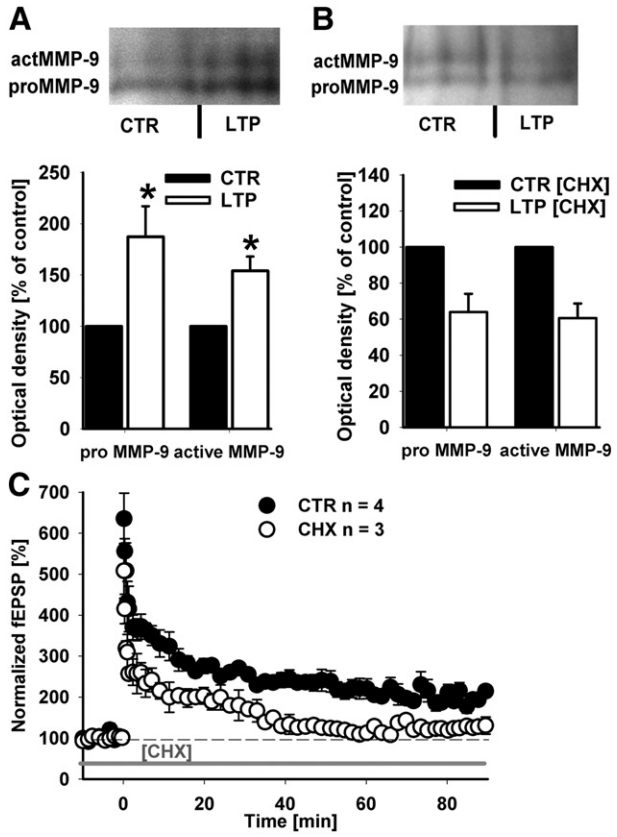

Fig. 3. LTP induction in the mf-CA3 pathway induces *de novo* expression of MMP-9. A, Gel zymography reveals an LTP-induced upregulation of pro- and active form of MMP-9 in homogenates from slice fragments containing mf-CA3 projection. B, Upregulation effect was abolished when LTP was induced in the presence of protein synthesis inhibitor (cycloheximide 60 μM). C, Averaged time course of fEPSP (normalized to the mean baseline fEPSP amplitude) in experiments in which LTP in the mf-CA3 pathway was induced (time t = 0 indicates LTP induction). Note that in control slices (filled circles), stable fEPSP increase is observed while in the presence of protein synthesis inhibitor (60 μM cycloheximide, bar), such a stable fEPSP enhancement is nearly abolished within 30–45 min (open circles).

MMP-9 immunohistochemistry

ISZ data (Fig. 1) may suggest that increased cytoplasmic DQ-gelatin fluorescence in the slices from LTP group might result from upregulation of MMP-9 protein. To provide additional support for this possibility, we have used immunohistochemistry in control and LTP slices. Importantly, the immunohistochemical MMP-9 staining apparently overlapped with the cell bodies (Fig. 4A–C). Moreover, LTP induction gave rise to a significant increase in the MMP-9 immunoreactivity both in the hilus and in the CA3 region (IRS values were 2.8 ± 1.4 and 4.7 ± 1.9 for control and LTP in the hilus, respectively and 2.0 ± 1.1 and 5.6 ± 3.0 for control and LTP in CA3, respectively, Dako anti-MMP-9 antibody, Fig. 4D). Similar results were obtained for the Santa Cruz anti-MMP-9 antibody (IRS values were 2.0 ± 0.8 and 3.1 ± 1.7 for control and LTP in the hilus, respectively and 2.1 ± 1.07 and 4.3 ± 1.6 for control and LTP in CA3, respectively, Santa Cruz anti-MMP-9 antibody, Fig. 4D). These immunohistochemical data are thus consistent with *in situ* zymography and provide an additional indication that MMP-9 might have been responsible, at least in part, for increased cytoplasmic DQ-gelatin fluorescence following LTP induction.

Active MMP-9 contribute to cytoplasmic gelatinolytic activity after LTP induction in neurons

MMPs are produced as inactive, latent enzymes and their activation requires the proteolytic removal of a pro-peptide sequence or chemical modification of inhibitory cysteine residue interacting with catalytic site according to "cysteine switch" hypothesis. Therefore, identification of MMP activity using *in situ* zymography may reveal only a fraction of active proteases and does not provide information about the pool of inactive protein in the latent form or enzymes associated with inhibitors e.g. TIMPs (tissue inhibitor of metalloproteinases) (Frederiks and Mook, 2004). Moreover, as already mentioned, in the ISZ, gelatinases present in their latent form might contribute to the gelatinolytic signal (Bannikov et al., 2002) but the extent of their contribution is *a priori* unknown. As an attempt to reveal the latent gelatinase pool in our preparation we have additionally performed *in situ* zymography in the presence of MMP activator APMA (Mungall and Pollitt, 2001). As shown in Fig. 5A, treatment of slices with this compound resulted in a strong increase in the gelatinolytic activity at neuronal soma and in the apparent extracellular space (Fig. 5A). More detailed quantification of confocal images revealed that in CTR slices, APMA treatment significantly increased mean DQ-gelatin fluorescence in the neuronal cytoplasm (1411 ± 99 AU) compared to buffer treated slices (614 ± 93 AU, $n=5$, $p<0.05$, images were acquired with identical settings). Interestingly, such an increase in fluorescence upon AMPA treatment was also observed in LTP group (1415 ± 132 AU vs. 943 ± 88 AU in APMA and buffer treated slices, respectively, $n=5$, $p<0.05$). Thereby, APMA caused comparable absolute increase in DQ-gelatin fluorescence in LTP and in control group (two way ANOVA for comparison of APMA-induced changes in fluorescence in control and LTP group, $p=0.2$). In contrast to cytoplasm, treatment with APMA decreased DQ-signal in neuronal nuclei in CTR slices (1457 ± 106 vs.

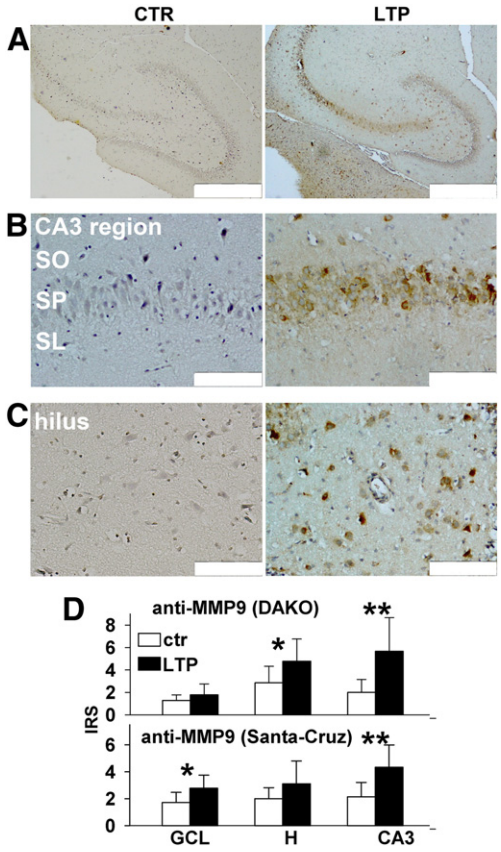

Fig. 4. Immunohistochemical staining indicates that LTP in mf-CA3 is associated with increased MMP-9 immunoreactivity in CA3 and hilar regions. A, Low magnification (40×) images of representative control section (left) and analogous section 2 h post LTP induction in mf-CA3 pathway (right). The sections were immunostained against MMP-9 (Dako anti-MMP9 antibody, brown color) and counterstained with haematoxylin to visualize nuclei (blue color). Note the increased immunoreactivity along mf-CA3 pathway after LTP induction. Scale bar — 500 μm. B–C, higher magnification (200×) of the CA3 region (B) and hilus (C) of the images presented in A. Note increased immunoreactivity in the cytoplasm of CA3 and hilar neurons associated with mf-CA3 LTP. SO-*stratum oriens*, SP-*stratum pyramidale*, SL-*stratum lucidum*. Scale bar — 100 μm. D, summary of MMP-9 immunoreactivity evaluation based on the semi-quantitative IRS (immuno-reactive score) scale in control (white bars) and LTP (black bars) sections obtained for DAKO (top) and Santa Cruz (bottom) anti-MMP9 antibodies ($n=9$ and 7 slices for LTP and control groups, respectively). Asterisk indicates statistical significance (* $p<0.05$, ** $p<0.001$, Mann–Whitney test).

3096 ± 159 AU in APMA and buffer treated slices, $n=4$, $p<0.05$), probably due to auto-degradation of the active enzyme. Similar to CTR group, in LTP slices, APMA decreased DQ-gelatin signal in the nuclei (2662 ± 240 AU vs. 3425 ± 164 AU in APMA and buffer treated slices, respectively, $n=5$, $p<0.05$). Notably, APMA treatment decreased nuclear gelatinolytic activity to a larger extent in LTP than in CTR slices (two way ANOVA, $p<0.001$). In the case of apparent extracellular signal, mean DQ-gelatin fluorescence after APMA treatment was significantly increased only in LTP group slices (329 ± 23 AU vs. 178 ± 60 AU in AMPA and buffer treated slices, respectively, $n=5$, $p<0.05$). Altogether, these data indicate that somata of CA3 neurons contain a prominent quantity of latent gelatinases.

Another issue that cannot be resolved basing solely on the *in situ* zymography are contributions of MMP-2 and MMP-9 to the gelatinolytic activity at various subcellular localizations of neuronal cells. We have approached this problem by immunostaining with specific antibodies for MMP-9 and MMP-2. MMP-9 immunoreactivity (Abcam antibody, ab38898) was detected in the soma and proximal dendrites of MAP-2 positive neurons (LTP group) in hilus and in the CA3 pyramidal layer (Fig. 5B). This signal shows a high degree of colocalization with gelatinolytic activity in neuronal soma (mean Mander's overlap coefficient 0.83 ± 0.01; $n=5$ sections from LTP group, for each 15–30 MAP-2 positive soma were analyzed after background adjustment in *stratum pyramidale* of CA3 region). Interestingly, at variance to *in situ* zymography, nuclear MMP-9 immunostaining showed a similar intensity to that observed in the cytoplasm (Fig. 5B). A qualitatively similar pattern of staining was obtained using a different MMP-9 antibody (Torrey Pines, TP221; data not shown).

Because in our hands two separate antibodies (Torrey Pines Biolabs, cat nr TP220 and Novocastra, cat. nr NCL-MMP2-507) against MMP-2 did not stain alcohol fixed tissue without antigen retrieval procedure (including boiling step) it was not possible to combine *in situ* zymography with MMP-2 immunostaining on the same section. Nevertheless, after antigen retrieval, MMP-2 immunoreactivity was present in MAP-2 positive neurons but in contrast to MMP-9, it was clearly more intense in nucleus than in the cytoplasm (Fig. 5C). Moreover, the overall MMP-2 immunostaining of CA3 neurons was markedly weaker than that for MMP-9 (compare Fig. 5B and C). In addition, MMP-2 staining was clearly localized in processes and nuclei of GFAP (glial fibrillary acidic protein) positive astrocytes (Fig. 5D).

MMP-9 but not MMP-2 is upregulated in nucleus and soma after LTP induction in mossy fiber — CA3 pathway

Since ISZ reveals the localization of all active enzymes able to digest gelatin, we have made an attempt to correlate the gelatinolytic activity with subcellular distribution of MMP-9 and MMP-2 in the MAP-2 positive neurons. To address this issue, we have immunostained thin sections against MMP-9 (Torrey Pines Biolabs, TP221) and MMP-2 protein (Torrey Pines Biolabs, TP220) and compared the distribution of immunofluorescent signal to that obtained using ISZ on sections from the same slices. To improve staining for MMP-9 and especially for MMP-2, we used antigen retrieval procedure before immunolabeling (see Experimental methods). As shown in Fig. 6, LTP induced a significant increase in MMP-9 signal-to-background ratio in the cytoplasm of MAP-2 positive neurons (4.12 ± 0.61 in LTP group, 2.55 ± 0.13 in control, $n=5$ slices, $p<0.05$). Apparent extracellular signal was similar in both groups (428.3 ± 48 AU in LTP, 469.5 ± 61 AU in control; $n=5$, $p>0.05$). In contrast to our results obtained with *in situ* zymography (Fig. 1), after LTP induction, we have observed a marked increase in the nuclear MMP-9 signal in neuronal CA3 nuclei (assessed as $F_{nucleus}/F_{ext}$ — nuclear to apparent extracellular space fluorescence ratio, 4.66 ± 0.21 vs. 2.89 ± 0.098 in LTP and control group, respectively, $n=5$, $p<0.001$).

Similar to CA3 region, LTP induction increased the cytoplasmic and nuclear MMP-9 level in the hilar MAP-2 positive neurons (average F_{int}/F_{ext} ratios for cytoplasm in LTP slices 3.77 ± 0.44 vs. 2.59 ± 0.13 in control, $p<0.05$ and for nuclei in LTP slices 4.44 ± 0.48 vs. 3.07 ± 0.19 in control, $p<0.05$; in each experiment $n=5$ slices) whereas signal associated with the apparent extracellular space was not significantly altered (428.9 ± 41 AU in LTP, 436.8 ± 44 AU in control, $n=5$, $p>0.05$, Supplemental Fig. S3).

Similar approach was applied to determine the subcellular distribution of MMP-2. In contrast to MMP-9, immunostaining against MMP-2 did not reveal any significant change in MMP-2 protein level after LTP induction in any of the considered cellular compartments: cytoplasm, nucleus and apparent extracellular region (Fig. 7). Altogether these data show that LTP induction in the mf-CA3 pathway upregulates MMP-9 but not MMP-2 protein level in CA3 and hilar neurons.

Discussion

The present data demonstrate that induction of LTP in the mf-CA3 pathway is accompanied by increased expression and enhanced

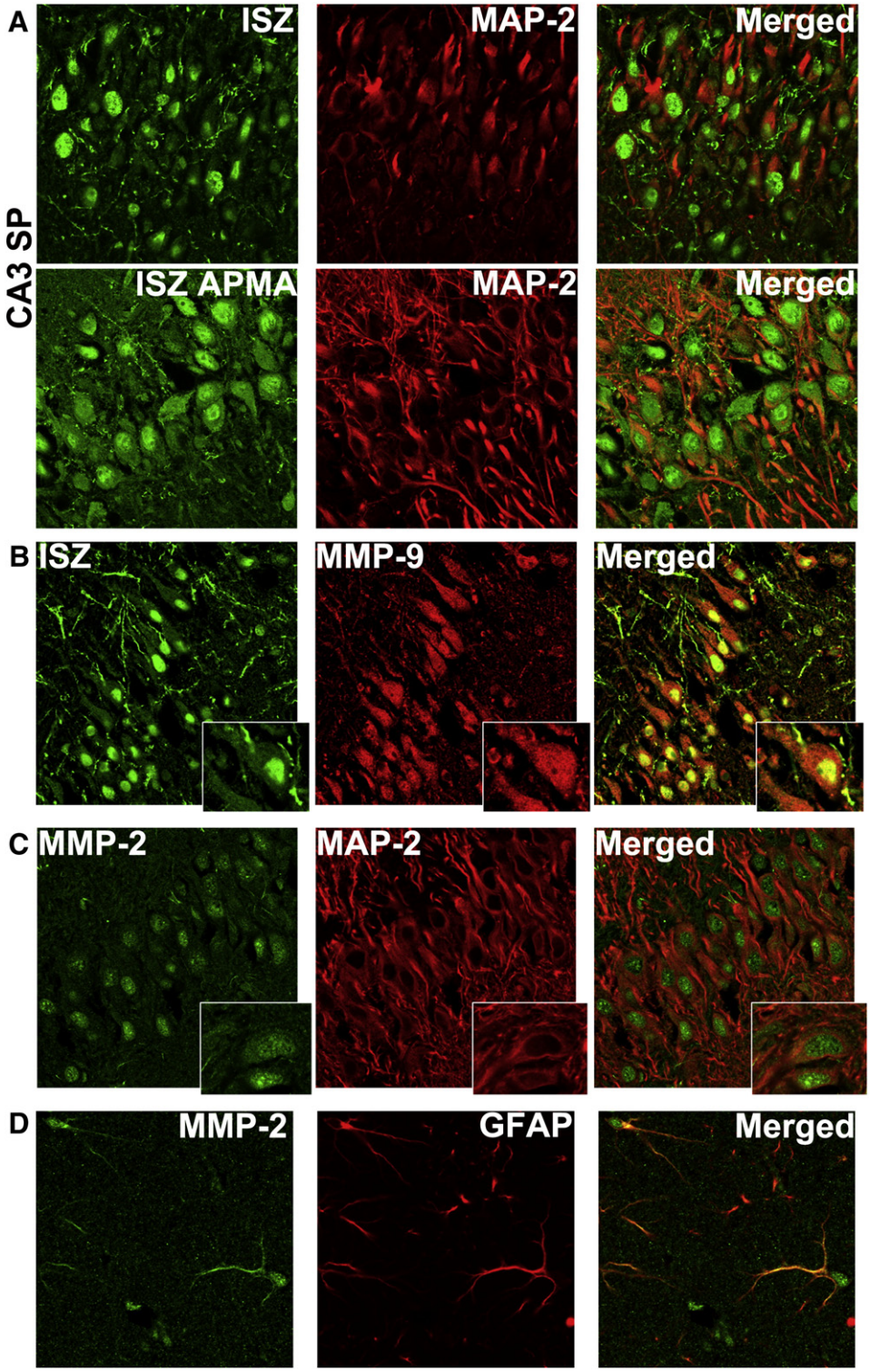

Fig. 5. Gelatinase activity localized in the cytoplasm and in apparent extracellular space colocalize mainly with MMP-9 but not with MMP-2 A, Incubation with APMA prior to *in situ* zymography increase DQ-gelatin fluorescence (green) in neuronal MAP-2 positive (red) soma and in apparent extracellular space. B, Double staining of *in situ* zymography (green) and MMP −9 immunofluorescence in CA3 pyramidal layer in LTP group. Note high degree of colocalization in neuronal cytoplasm as shown on insets. C, Typical examples of staining with MMP-2 (green) and the neuronal maker MAP-2 (red) in the hippocampal CA3 *stratum pyramidale*. Note MAP-2-positive pyramidal neurons with MMP-2 positive nuclei and weak, diffuse signal in neuronal cytoplasm. D, CA3 *stratum radiatum* staining with MMP-2 (green) and GFAP (red). Note that GFAP-expressing astrocytes are highly MMP-2 positive.

activity of gelatinases along this projection. The most novel and surprising observation is that LTP is associated with a strong upregulation of MMP-9 expression and increased gelatinases activity in the intracellular neuronal compartments. To the best of our knowledge this is the first observation that induction of synaptic plasticity is clearly correlated with the expression and function of gelatinases in the neuronal cytoplasm and nucleus. The analysis of the ISZ images also suggests that LTP induction enhances the gelatinolytic activity in the extracellular milieu but, as already mentioned, the diffuse signal in the apparent extracellular space might also result, at least in part,

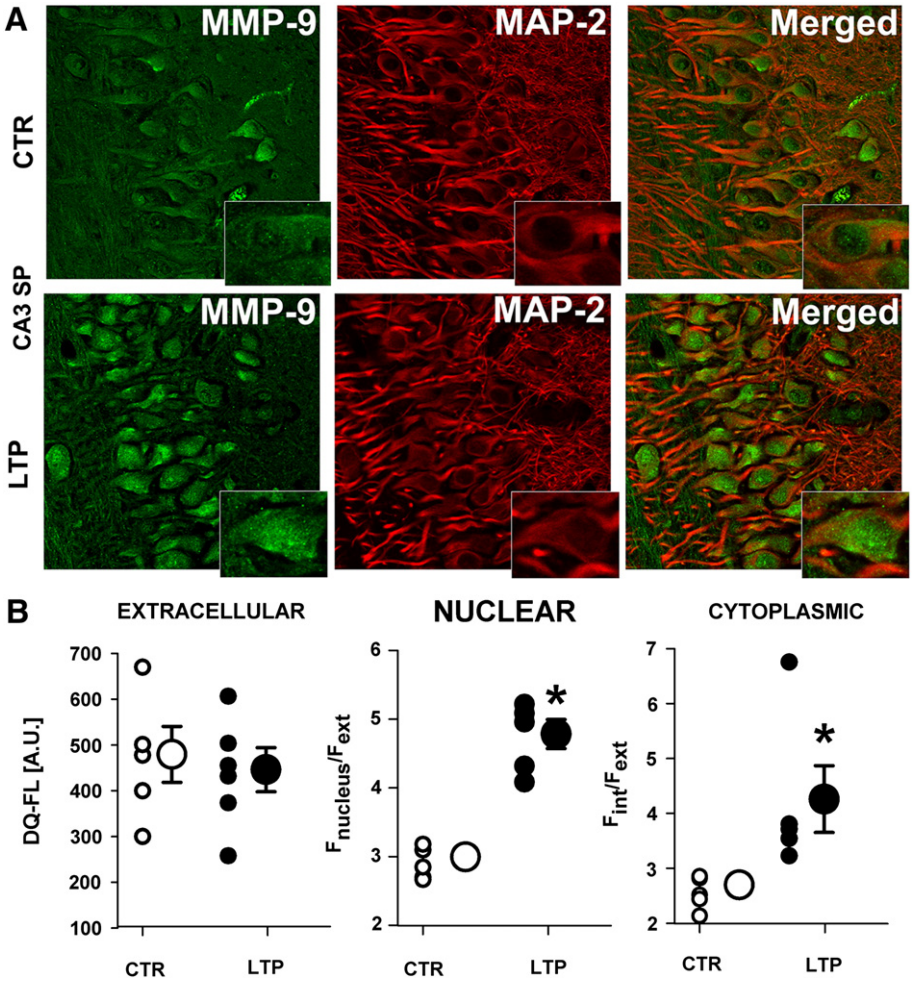

Fig. 6. LTP in mf-CA3 is associated with changes in MMP-9 level in neurons from CA3 region. A, Representative images of CA3 *stratum pyramidale* (CA3 SP) of control hippocampal slice (top row) and 2 h post LTP induction in mf-CA3 pathway (bottom row). Sections were stained against MMP-9 (green, Torrey Pines Biolabs, TP221) and counterstained with MAP-2 (red), a neuronal marker. Insets show soma of individual CA3 pyramidal neurons from the same section. Note increase in the cytoplasmic and nuclear fluorescence in LTP group. B, Statistics of MMP-9 fluorescence intensity for apparent extracellular space (AU), nuclear $F_{nucleus}/F_{ext}$ and cytoplasmic of CA3 *stratum pyramidale* neurons ($n = 5$ slices). Note that the distribution of mean fluorescence in neuronal nuclei and cytoplasm in LTP slices significantly differ from that in control slices in contrast to apparent extracellular signal.

from astrocytic, dendritic or oligodendrocytic structures (Gawlak et al., 2009). It is noteworthy, however, that secreted gelatinases operate pericellularly after association with specific cell surface receptors or cell-associated ECM molecules (CD44, proteoglycans, integrins) via hemopexin or fibronectin type II domains (Murphy and Nagase, 2011). Thus, after LTP induction, released MMPs could accumulate and thereby enhance the gelatinolytic signal in the extracellular space. However, their distribution and molecular targets in this compartment remain unknown and other hypotheses should be also considered (see below). Incomplete blockade of gelatinolytic signal by FN-439 (Fig. 2B) indicates that besides gelatinases, other enzymes could be involved in digestion of the DQ-gelatin. Markedly more effective signal blocking by other MMP inhibitors (phenanthroline and GM-6001) and the lack of effect of the serine protease inhibitor PMSF suggest involvement of other metzincins (Rivera et al., 2010). However, several lines of evidence indicate that predominant gelatinolytic activity in the cytoplasm and in the apparent extracellular space was due to gelatinases. Most importantly, the residual gelatinolytic activity following FN-439 treatment was almost exclusively localized in the nuclei (Fig. 2C). Moreover, there was a high degree of co-localization between gelatinolytic signal in the ISZ and immunofluorescent staining against MMP-9 in the cytoplasm (Fig. 5B). In addition, immunohistochemistry (Fig. 4) revealed a clear cytoplasmic MMP-9 staining resembling that observed in the ISZ and in the immunofluorescent labeling. Thus, our data indicate that the intracellular gelatinolytic signal in neurons was due to activity of gelatinases except for a residual nuclear signal which may result from some unidentified MMPs (e.g. MT1-MMP, Yang et al., 2010).

Immunofluorescent staining for MMP-9 and MMP-2 (Figs. 5, 6 and S3) provided an important information regarding their subcellular distribution and sensitivity to stimuli inducing LTP. Thus, MMP-9 is abundantly present in the cytoplasm, yielding a comparable staining intensity as in the nucleus (Fig. 5). This pattern of MMP-9 distribution is further supported by immunohistochemical staining (Fig. 4). In contrast, MMP-2 appears to be predominantly localized in the neuronal nuclei, although a faint cytoplasmic staining was also present and, as already observed (Szklarczyk et al., 2002), MMP-2 is particularly abundant in GFAP-positive astrocytes. Most importantly, our analysis indicates that only MMP-9 is upregulated following LTP induction in the mf-CA3 projection. This finding appears consistent with numerous reports in which MMP-9 has been implicated in the synaptic plasticity in other projections as well as in learning (Bozdagi et al., 2007; Meighan et al., 2006, 2007; Nagy et al., 2007; Okulski et al., 2007; Wang et al., 2008). Moreover, consistent with data on other models (Brown et al., 2008; Meighan et al., 2006; Nagy et al., 2006; Wright et al., 2003, 2006) we found no correlation between synaptic plasticity and expression of MMP-2 (but see Mizoguchi et al., 2007).

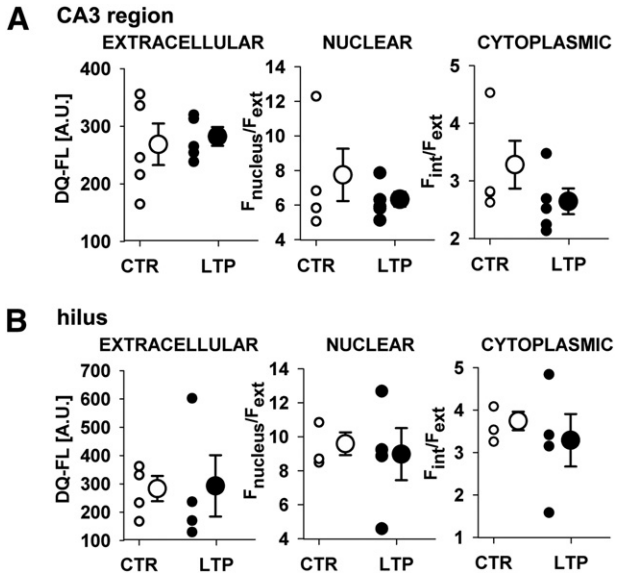

Fig. 7. LTP induction in mf-CA3 is not associated with changes in MMP-2 immunofluorescence in CA3 ad hilar neurons. A, Statistics of MMP-2 fluorescence intensity of apparent extracellular space (AU), nuclear ($F_{nucleus}/F_{ext}$) and cytoplasmic (F_{int}/F_{ext}) compartments of CA3 *stratum pyramidale* neurons in control slices and 2 h after LTP induction in mf-CA3 pathway ($n=5$). B, Statistics of MMP-2 fluorescence intensity of apparent extracellular space (AU), nuclear ($F_{nucleus}/F_{ext}$) and cytoplasmic (F_{int}/F_{ext}) compartments of hilar neurons in control slices ($n=3$) and 2 h after LTP induction in mf-CA3 pathway ($n=4$). Note lack of any statistically significant differences in MMP-2 level between control and LTP group both in CA3 and hilus.

When interpreting the results obtained with ISZ it needs to be considered that a small but *a priori* unknown part of the DQ-gelatin fluorescence might be due to the activity of gelatinases in their latent form (Bannikov et al., 2002). In practice, this implies that the gelatinolytic activity detected in the ISZ cannot be ascribed exclusively to gelatinases in their active form prior to fixation. Our data obtained using gel zymography indicated that both active and latent form of MMP-9 are upregulated following LTP induction, raising a possibility that increased gelatinolytic signal and MMP-9 level in the cytoplasm might be due to *de novo* protein synthesis. However, it should be stressed that the gel zymography data were obtained on homogenized tissue and increased expression of MMP-9 in specific cellular compartments (e.g. in cytoplasm) requires additional evidence. This problem cannot be elucidated using immunohistochemical or immunofluorescent staining as antibodies used here do not distinguish between active and latent forms of gelatinases. Importantly, APMA strongly enhances the DQ-gelatin fluorescence (Fig. 5A), revealing a large pool of inactive (presumably latent) gelatinases. This observation provides an indirect indication that, in our model, latent gelatinases show a weak efficiency in digesting the DQ-gelatin and, therefore, the gelatinolytic signal is likely to result predominantly from the enzymes in their active form. Moreover, APMA does not activate MMP-9 when it is associated with TIMP-1 (Ogata et al., 1995) which suggests that increased DQ fluorescence observed after treatment with this compound (Fig. 5A) is related to the intracellular pool of MMP-9 which is not associated with TIMP-1. Whatever is the contribution of the active and latent gelatinase forms to the observed DQ-gelatin fluorescence, these observations indicate that the intracellular and extracellular reservoir of gelatinases may be considerably larger than that detected using the ISZ. Intriguingly, while ISZ did not reveal any enhancement of the nuclear signal after LTP induction (Fig. 1F), immunolabeling clearly indicated an increase in the nuclear MMP-9 signal both in CA3 and hilus (Figs. 6 and S3). A likely explanation for this discrepancy could be that LTP induction results in *de novo* expression of latent MMP-9 or MMP-9 associated with TIMPs which are probably "invisible" for the ISZ technique but can be detected by immunostaining. However, the use of APMA gave rise to a reduction of the nuclear gelatinolytic signal. We may speculate that this was due to an auto-degradation or digestion by other MMPs in their active form which, judging from our ISZ and immunostaining, are highly concentrated in the nuclei favoring these processes. In the context of reported here abundant nuclear MMP-9 pool it is worth mentioning that, intriguingly, this gelatinase lacks the nuclear localization signal (Cauwe and Opdenakker, 2010). The mechanisms responsible for its translocation to the nucleus remain to be elucidated.

In contrast to the nucleus, in the apparent extracellular space, ISZ revealed a larger gelatinolytic signal in the LTP group than in controls while immunofluorescent labeling for MMP-9 and MMP-2 did not show any significant difference in this compartment (both in CA3 and hilus, Figs. 6, 7 and S3). This finding suggests an alternative scenario with respect to that discussed above (accumulation of released gelatinases). Namely, it seems that LTP induction results primarily not in the increase in the amount of protein but rather in activation of latent MMP-9 already present in the extracellular compartment. Extracellular MMP-9 could be activated by NO and/or by proteolytic cleavage by tPA/plasmin system or other MMP (Sang et al., 1995; Wang et al., 2011). As already explained, the apparent extracellular space could contain several cellular structures including neuropil or glial processes. It cannot be excluded that following LTP induction, MMP-9 is released from these compartments and activated, yielding thus enhanced proportion of active MMP-9 while the total MMP-9 pool in the "apparent extracellular space" would remain unchanged. Altogether, these results indicate that within 2 h after induction, LTP differentially affects MMP-9 in the considered compartments: in the nuclei the latent form is increased, in the cytoplasm — both latent and active forms are upregulated while in the apparent extracellular space LTP appears to stimulate the conversion of the latent form of this gelatinase into the active one.

Our results based on the gel zymography (Fig. 3A,B) indicate that LTP induction in the mf-CA3 pathway is accompanied by a rapid (within 2 h), protein synthesis-dependent increase in both activity and expression level of MMP-9 which is further supported by increased immunofluorescent (Figs. 6 and S3) and immunohistochemical (Fig. 4) MMP-9 staining. Although appearance of such a substantial amount of newly synthesized proteins might be surprising, it has been previously reported that increase in MMP-9 level in response to plasticity evoking stimuli does take place. Nagy et al. (2006) have observed a transient increase in active MMP-9 reaching the peak as early as 30 min after application of an agent eliciting chemical LTP in the CA1 hippocampal area. Moreover, in the model of kainate-induced tissue remodeling, MMP-9 RNA and protein was enhanced within hours after kainate administration (Szklarczyk et al., 2002). It seems thus that, indeed, stimuli eliciting plasticity or remodeling of neuronal networks are able to induce a rapid and effective MMP-9 protein synthesis. Additional indication for importance of the *de novo* synthesized MMP-9 protein in the context of the mf-CA3 synaptic plasticity is provided by our experiments with CHX which abolished the LTP consolidation (Fig. 3C) as well as the upregulation of both MMP-9 forms (Fig. 3A,B). Interestingly, in the presence of CHX, the return of fEPSP to the baseline after the post-tetanic potentiation was relatively rapid (Fig. 3C) strongly resembling that observed in the presence of MMP blocker (FN-439, Fig. 2A in Wojtowicz and Mozrzymas, 2010). These results thus reinforce the notion that LTP maintenance in the mf-CA3 pathway critically depends on MMP-9 which is rapidly upregulated following application of plasticity-inducing stimuli.

Interestingly, the upregulation of MMP-9 expression in the mf-CA3 pathway did not require the activity of NMDARs, as all experiments were carried out in the presence of APV (to suppress potentiation originating from non-mossy fiber synapses, Figs. 3, 4). This is in contrast to previous reports on Sch-CA1 projection in which a crucial

role of NMDARs in the LTP-induced MMP expression was emphasized (Nagy et al., 2006; Meighan et al., 2007). These findings indicate that although in both pathways, LTP induction upregulates MMP expression and activity, the underlying molecular mechanisms may be profoundly different.

Although MMPs are best known for their role in the proteolysis of extracellular protein targets, growing evidence indicates intracellular localization of these enzymes in neurons, including nucleus (Foscarin et al., 2011; Yang et al., 2010) and cytoplasm (Choi et al., 2011; Cuadrado et al., 2009; Szklarczyk et al., 2007). The present work provides further evidence for abundant presence of intraneuronal MMPs and raises a fundamental question regarding the specific role of the intracellular MMP-9 (both cytoplasmic and nuclear) in the maintenance of synaptic plasticity. As already mentioned, MMPs are traditionally regarded as enzymes which are rapidly secreted as inactive precursors (Rivera et al., 2010) and operating extracellularly following their activation (Hwang et al., 2005; Michaluk et al., 2007; Tian et al., 2007). Thus, the presence of latent MMP-2/9 in the cytoplasmic compartments is not unexpected as these proteins are likely to represent MMPs which are newly synthesized and prepared for secretion. The most surprising finding of this work is that neuronal cytoplasm contains an abundant pool of active gelatinases (predominantly MMP-9) which is further enriched after LTP induction. This observation points to a novel role of intracellular pool of MMP-9 protease as a potential regulator of mechanisms underlying synaptic plasticity. As we mentioned in the Introduction, gelatinases have been distinguished as those MMPs which target numerous putative intracellular substrates (Cauwe and Opdenakker, 2010). For instance, Yang et al. (2010) indicated two nuclear proteins poly-ADP-ribose polymerase-1 (PARP-1) and X-ray cross-complementary factor 1 (XRCC1) as MMP-2/9 substrates and hypothesized that gelatinase-dependent PARP-1 and XRCC1 cleavage might interfere with oxidative DNA repair. It is worth noting that functional PARP-1 protein was implicated in the long-term plasticity (Cohen-Armon et al., 2004; Hernandez et al., 2009). In the context of the present study it is thus tempting to speculate that MMP-9 dependent PARP-1 processing could be involved in the LTP maintenance in the mf-CA3 pathway. Henninger et al. (2007) has used proteomic tools to detect changes in cytosolic proteins level after spatial learning in the hippocampus and, strikingly, several proteins altered by this learning paradigm are also implicated as putative substrates of intracellular gelatinases (fascin, RHOGDI-1 or elongation factor-2, Cauwe and Opdenakker, 2010). It is thus possible that the potential reduction in the level of some intraneuronal proteins during spatial learning is caused by MMP-dependent cleavage.

In conclusion, we provide the first evidence that induction of LTP in the mf-CA3 pathway is associated with enhanced activity as well as increased level of intracellular MMP-9 while MMP-2 is not affected. Although the spatial distribution of MMPs in the extracellular space will require a separate analysis, our data suggest that after LTP induction, the pool of active extracellular MMP-9 may also be enriched. Research to date has described intracellular MMP activity in the context of pathological processes such as ischemia, Parkinson disease or synaptic atrophy (Cauwe and Opdenakker, 2010). The present work provides the first evidence that intracellular gelatinases activity may play an important role in physiological processes related to synaptic plasticity and cognition.

Experimental methods

Hippocampal slice preparation and electrophysiology

Wistar rats (P32–P52) were anesthetized with isoflurane and decapitated. All procedures were approved by Local Ethic Commission and an effort was made to minimize the number of animals used for experiments. The brain was quickly removed and transverse slices (400 μm thick) were cut with a vibratome (Leica VT1200S, Germany) in ice-cold buffer containing (in mM): sucrose 75, NaCl 87, KCl 2.5, NaH_2PO_4 1.25, $NaHCO_3$ 25, $CaCl_2$ 0.5, $MgCl_2$ 7, and glucose 20, oxygenated by saturation with carbogen (95% O_2, 5% CO_2), pH 7.4. Slices were transferred to a chamber containing the same carbogen saturated solution and kept at 32 °C for 20 min. Slices were then maintained in a holding chamber at room temperature in oxygenated artificial cerebrospinal fluid containing (in mM): NaCl 125, $NaHCO_3$ 25, KCl 2.5, NaH_2PO_4 1.25, $CaCl_2$ 2.5, $MgCl_2$ 1, glucose 20, pH 7.4 for at least 1 h. Synaptic transmission in the mossy fiber pathway was investigated as described previously (Wojtowicz and Mozrzymas, 2010). LTP was evoked by tetanic stimuli (4×100 Hz, 1 s with 10 s intervals). Field excitatory postsynaptic potentials (fEPSP) signal was identified as originating from mossy fibers based on: a) a short latency (≤5 ms); b) high paired pulse facilitation ratio at 50 ms interval (≥1.5); c) high burst facilitation at 100 Hz (4th to 1st pulse amplitude ratio≥3.0; d) strong fEPSP signal suppression (at least 80%) by mGluR group II agonist 2-(2,3-dicarboxycyclopropyl) glycine (DCG-IV, 1 μM, Tocris Bioscience, UK) applied at the end of each experiment. All recordings were made at 30–31 °C in the presence of L-APV (25 μM, Tocris Bioscience, UK), the NMDA receptor blocker. Results related to fEPSP concern the amplitude of these signals.

Tissue preparation

For zymography and immunofluorescent staining, brain slices (400 μm-thick) were immersed in alcoholic fixative (1 methanol:3 ethanol 95%) for 20 min at 4 °C and subsequently kept at −20 °C. Fixed slices were washed in 99.8% ethanol (4 °C) and processed through several mixtures of ethanol and increasing concentration of polyester wax (Science Services, Germany) until slices were embedded in pure wax. For immunochemistry use, transverse hippocampal slices were fixed in 5% buffered formalin, dehydrated and embedded in paraffin. All tissue preparations were cut into 4 μm-thick sections on rotary microtome (Leica, RM 2255, Germany) and mounted on glass slides (Superfrost Plus slides, Menzel Glaser, Germany).

Immunohistochemistry — IHC

Four micrometer tissue sections were deparaffinized with xylene and gradually rehydrated. Activity of endogenous peroxidase was blocked using 3% hydrogen peroxide. Immunohistochemical reactions were performed using anti-MMP-9 antibodies: against protein C terminus (Santa Cruz, USA, cat. nr sc-6840) and N terminus (Dako, Denmark, cat. nr A0150) and conducted overnight at 4 °C. Following incubation with secondary biotinylated antibodies (Biotinylated Link), reactions with the streptavidin-biotinylated peroxidase complex (LSAB + System-HRP) were performed. The peroxidase substrate of 3,3′-diaminobenzidine (DAB + Chromogen) was used as a chromogen. All sections were counterstained with haematoxylin. All reagents were from Dako (Denmark). The intensity of MMP-9 expression was evaluated using the semi-quantitative IRS (immuno-reactive score) scale according to (Remmele and Stegner, 1987) which took into account the intensity of the color reaction and the percentage of positive cells. The final score represents a product of points given for individual traits and ranged between 0 and 12. In every case the appraisal was performed in five representative microscope fields (hotspot, 200×). Intensity of immunohistochemical reactions was evaluated independently by two pathologists in a blind fashion.

In situ zymography — ISZ

In situ zymography was performed according to Gawlak et al. (2009), with modifications. Tissue sections were dewaxed in 99.8% ethanol and rehydrated directly with distilled water. Next, hippocampal sections were preincubated with tap water (37 °C, 90 min) and

subsequently were covered with a fluorogenic substrate — DQ-gelatin for 80 min at 37 °C (1:100 dilution in manufacturers buffer, Invitrogen, USA). Finally, substrate was washed out with Tris buffer saline with 0.025% Triton X-100 (TBS-Tx) and glass slides were mounted with Fluoroshield (Sigma, cat. nr F6182) or additionally sections were probed with specific antibodies.

To identify proteases that might have contributed to DQ-gelatin fluorescence (see Results), different inhibitors were used during the whole slice processing (hydratation, reaction with DQ-gelatin and washing). The proteases inhibitors were used at the following concentrations: serine protease inhibitor PMSF (phenylmethylsulfonyl fluoride, 0.2–1 mM), MMP pan-inhibitors phenanthroline (10 mM), GM-6001 (1 mM) and FN-439 (0.5–5 mM). In a series of experiments, latent gelatinases were activated prior to zymography by incubating the slices with 1 mM APMA (4-aminophenyl mercuric acetate) for 6 h (dissolved in TBS). Then slices were washed 3 times with TBS and ISZ procedure was performed. All chemicals were from Sigma-Aldrich except: FN-439 (Calbiochem, USA) and GM6001 (Chemicon, USA).

Immunofluorescence

Before MMP-9 and MMP-2 immunolabeling antigen retrieval procedures were applied. Dewaxed and rehydrated sections were incubated in buffer pH 6.0 or pH 9.0 (98 °C, 20 min, Target Retrieval Solution, Dako, Denmark). Then the slices were cooled down, washed 10 min with tap water and 30 s with deionized water. Sections were routinely blocked for 1 h with 20% normal horse serum (NHS, Vector Laboratories, USA). Afterwards, slices were incubated overnight at 4 °C with diluted primary antibodies and 2% NHS (anti-MAP-2, 1:500, Sigma, cat. nr M4403, anti-MMP-9, 1:500, Torrey Pines Biolabs, cat nr TP221; anti-MMP-2 1:250, Torrey Pines Biolabs, cat nr TP220; anti-GFAP, 1:500, Sigma-Aldrich, cat nr G3893). Subsequently, slices were incubated for 2.5 h at RT with diluted secondary antibodies (AlexaFluor 633 goat anti-mouse, 1:2000 and AlexaFluor 488 goat anti-rabbit, 1:2000, Invitrogen). Finally, glass slides were mounted with Fluoroshield. For NHS and antibody dilution we used TBS-0.1% Triton X-100 buffer. Between each step of immunostaining procedure, sections were washed with TBS-Tx. In the case of FL staining following zymography, the step of antigen retrieval was omitted, and replaced with postfixation procedure. Sections after ISZ were incubated in 4% paraformaldehyde and 0.2% picric acid in 0.1 M phosphate-buffered saline (pH 7.4, 15 min, RT), then washed and followed with antibody staining procedure.

Image acquisition

Wide-field fluorescence was acquired with NiR Apo 40×0.8 NA water immersion objective and Nikon DSQi1Mc 1.3Mpix CCD camera (Nikon Eclipse FN1 microscope, Nikon, Japan). For wide-field fluorescence microscopy, a particular care was taken that pairs of control and LTP slices from the same animal were processed simultaneously and subsequently imaged with identical acquisition parameters (i.e. camera gain, exposition time). DQ fluorescence associated with neuronal cytoplasm was analyzed in the same set of sections in images obtained with laser scanning confocal microscope (PlanApo 60×1.35 NA oil immersion objective, Olympus Fluoview1000S microscope, Olympus, Japan). A series of 0.4 μm optical sections (z-stack, 3–4 μm in depth) were acquired for each field of view (approximately 200×200 μm) and subsequently sum-projected. For more reliable quantification of faint DQ fluorescence associated with cytoplasm and "apparent extracellular" compartment (see below), the confocal images were acquired in such a way that DQ fluorescence associated with neuronal nuclei was overexposed during image acquisition and excluded from further analysis. This approach enabled us to more optimally adjust the dynamic range of our 8-bit photomultiplier (256 gray levels scale) to detect with higher resolution subtle changes in DQ fluorescence between compartments.

Image analysis

The image analysis was performed in the following steps. First, areas of 3–5 adjacent visual fields (approximately 200×180 μm each) for hilus or CA3 regions were analyzed within each thin (4 μm) section and the data were pooled. Next, the measurements were repeated in 2–3 other serial sections from the same slice. Finally, average values of all sections were pooled providing a reliable value of average DQ fluorescence of one thick (400 μm) slice used in electrophysiological experiment. Such analysis was performed in hippocampal sections stained against microtubule associated protein 2 (MAP-2), a neuronal marker. In our hands, MAP-2 antibody stained both soma and dendrites of rat hippocampal neurons (see Fig. 1A) and therefore it was used as a reference of neuronal structure in computer- and visually-guided image analysis in Nis-Br Elements (Nikon, Japan) and ImageJ (http://rsb.info.nih.gov/ij/) software. The analysis of cytoplasm- and nuclei-associated DQ fluorescence was performed within regions of interest (ROIs) exclusively in MAP-2 positive cells (i.e. neurons) of CA3 *stratum pyramidale* and hilar region.

Total DQ fluorescence in the hilus or CA3 region was calculated based on mean fluorescence of 3–5 consecutive images (fields of view) acquired with wide-field microscopy (weighted average of all 1.3 M pixels in each image, ImageJ software). Fluorescence intensity for neuronal nuclei and background fluorescence ("apparent extracellular", see below) was also calculated from images acquired in wide-field mode, while cytoplasm fluorescence was calculated in confocal mode. Briefly, neuronal nuclei were analyzed based on the characteristic oval shape and high fluorescence intensity (see Fig. 1A). Some of the slices were additionally stained against nuclear marker DAPI to show the appropriate apposition between DAPI-positive nuclei and ROI position (Supplemental Fig. S1). Fluorescence in the area surrounding the neuronal cell bodies in CA3 region (i.e. *strata lucidum* and *oriens*) or hilus was analyzed in the following steps: 1) 3D plot of DQ fluorescence intensity was visually inspected to determine the localization of both minimal fluorescence (typically associated with tissue discontinuities) and intense fluorescence associated with nuclei and structures in the neuropil or other cellular structures (Interactive 3D surface plot by Kai UweBarthel, ImageJ software), 2) the image fluorescence intensity histogram was probed with threshold tool in such a way that only pixels whose intensity could not be described with the above mentioned criteria and were not associated with MAP-2 positive neuronal cell bodies were selected, 3) the weighted average of fluorescence in the highlighted pixels was calculated (Fig. 1B). This approach enabled us to indicate the area of homogenous fluorescence not associated with neuronal cell bodies, proximal dendrites or tread-like oligodendrocyte processes (Gawlak et al., 2009). For the purpose of this study, the fluorescence quantified in this way in each field of view is described as "apparent extracellular" DQ fluorescence in contrast to cytoplasmic and nuclear compartments. It needs to be emphasized that "apparent extracellular region" is used here as a purely technical term — we are aware that it might cover some cellular or subcellular structures. DQ fluorescence of the cytoplasm for each neuron (F_{int}, nuclear signal excluded) was quantified in confocal images. Because of the different acquisition requirements comparing to wide-field fluorescence (see above), F_{int} was normalized to average apparent extracellular fluorescence (F_{ext}) in each image and expressed as F_{int}/F_{ext} ratio.

In the case of experiments with protease inhibitors representative confocal images of DQ-gelatin-treated sections were obtained and weighted mean fluorescence was measured in CA3 stratum pyramidale.

Mander's overlap coefficient was used for colocalization analysis with Intensity Correlation Analysis plugin in ImageJ software.

Gelatin zymography

Dentate gyrus and field CA3 were isolated together from hippocampal slices after the electrophysiological experiments (ca. 2–3 h after tetanus induced LTP in mf–CA3 pathway, LTP group) then frozen and stored. Control group was collected in an analogous manner but slices were subjected to the baseline stimulation only (2–3 h). Protein extraction was performed according to Szklarczyk et al. (2002) and Zhang and Gottschall (1997) with some modifications. Tissue homogenization was performed in ice-cold 50 mM Tris-Cl buffer with 10 mM $CaCl_2$, 0.25% Triton X-100 and 0.1 mM PMSF (30 μl buffer/ 1 mg wet tissue). Homogenate was centrifuged at 6000×*g* for 30 min at 4 °C. Pellet containing Triton X-100 poor-soluble proteins was resuspended in 50 mM Tris-Cl buffer, pH 7.4 with 2% Triton X-100, 0.1 M $CaCl_2$, incubated 12 min in 60 °C and centrifuged (30 min, 10,000 ×*g*, 4 °C). Supernatant containing extracellular matrix and membrane associated proteins was precipitated with 60% cold ethanol and centrifuged (10 min, 14,000 ×*g*, 4 °C). Pellets were solubilized in non-reducing SDS-sample buffer without boiling. Protein concentrations were measured using Bicinchoninic Acid Protein Assay Kit (Thermo Scientific, USA) in samples before ethanol precipitation. Equal amounts of proteins were separated in non-reducing conditions on 8% SDS-PAGE gel co-polymerized with 2%-fish skin gelatin (Sigma-Aldrich, Germany). Gels were washed in 2.5% Triton X-100 (2×30 min). Enzymatic reactions were performed in buffer containing 50 mM Tris, pH 7.5, 10 mM $CaCl_2$, 1 μM $ZnCl_2$, 1% Triton X-100, 0.02% sodium azide with continuous mixing at 37 °C for 3–5 days. Gels were stained with 0.1% Coomassie Blue G-250 for 2 h and distained with 5% acetic acid until clear white proteolytic bands appeared on the blue background. Additionally, the same samples were resolved in parallel SDS-PAGE gel without gelatin to verify protein load across samples. Gels were digitally photographed (Geldoc1000 system, Bio-Rad, USA) and gelatinolytic activity was quantified with ImageJ (NIH, USA).

Statistical analysis

Statistical analysis was performed with SigmaStat software (SyStat, USA). Densitometric data from gelatin substrate gel zymography were analyzed by ANOVA with Tukey post hoc multiple comparison test. Mean fluorescence values throughout this study were compared using unpaired student *t*-test. In case of immunohistochemistry Mann–Whitney *U* test was applied. Cumulative histograms were compared with Kolmogorov–Smirnov (K-S) test. K-S statistics refers to maximal vertical deviation between analyzed distributions. All data are presented as mean ± SEM with significance levels of: $^{*}p<0.05$, $^{**}p<0.01$. *n* refers to the number of slices each of which was representing a different animal.

Supplementary materials related to this article can be found online at doi:10.1016/j.mcn.2012.04.005.

Acknowledgements

This work was supported by the Polish Ministry for Science and Higher Education grant No. N401 541540 and partially supported by PN/030/2006. T. W. was additionally supported by "Iuventus Plus" grant IP2010_047870, research fellowship within "Development program of Wroclaw Medical University" funded from the European Social Fund, Human Capital, national Cohesion Strategy" (contract no. UDA-POKL.04.01.01-00-010/08-00)" and Stipend for Young Researchers START from Foundation for Polish Science.

References

Acsady, L., Kamondi, A., Sik, A., et al., 1998. GABAergic cells are the major postsynaptic targets of mossy fibers in the rat hippocampus. J. Neurosci. 18, 3386–3403.

Bannikov, G.A., Karelina, T.V., Collier, I.E., et al., 2002. Substrate binding of gelatinase B induces its enzymatic activity in the presence of intact propeptide. J. Biol. Chem. 277, 16022–16027.

Bozdagi, O., Nagy, V., Kwei, K.T., et al., 2007. In vivo roles for matrix metalloproteinase-9 in mature hippocampal synaptic physiology and plasticity. J. Neurophysiol. 98, 334–344.

Brown, T.E., Forquer, M.R., Harding, J.W., et al., 2008. Increase in matrix metalloproteinase-9 levels in the rat medial prefrontal cortex after cocaine reinstatement of conditioned place preference. Synapse 62, 886–889.

Butler, G.S., Overall, C.M., 2009. Updated biological roles for matrix metalloproteinases and new "intracellular" substrates revealed by degradomics. Biochemistry 48, 10830–10845.

Calixto, E., Thiels, E., Klann, E., et al., 2003. Early maintenance of hippocampal mossy fiber–long-term potentiation depends on protein and RNA synthesis and presynaptic granule cell integrity. J. Neurosci. 23, 4842–4849.

Cauwe, B., Opdenakker, G., 2010. Intracellular substrate cleavage: a novel dimension in the biochemistry, biology and pathology of matrix metalloproteinases. Crit. Rev. Biochem. Mol. Biol. 45, 351–423.

Cauwe, B., Van den Steen, P.E., Opdenakker, G., 2007. The biochemical, biological, and pathological kaleidoscope of cell surface substrates processed by matrix metalloproteinases. Crit. Rev. Biochem. Mol. Biol. 42, 113–185.

Choi, D.H., Kim, Y.J., Kim, Y.G., et al., 2011. Role of matrix metalloproteinase 3-mediated alpha-synuclein cleavage in dopaminergic cell death. J. Biol. Chem. 286, 14168–14177.

Cohen-Armon, M., Visochek, L., Katzoff, A., et al., 2004. Long-term memory requires polyADP-ribosylation. Science 304, 1820–1822.

Cuadrado, E., Rosell, A., Penalba, A., et al., 2009. Vascular MMP-9/TIMP-2 and neuronal MMP-10 up-regulation in human brain after stroke: a combined laser microdissection and protein array study. J. Proteome Res. 8, 3191–3197.

Ethell, I.M., Ethell, D.W., 2007. Matrix metalloproteinases in brain development and remodeling: synaptic functions and targets. J. Neurosci. Res. 85, 2813–2823.

Foscarin, S., Ponchione, D., Pajaj, E., et al., 2011. Experience-dependent plasticity and modulation of growth regulatory molecules at central synapses. PLoS One 6, e16666.

Franzke, C.W., Tasanen, K., Schacke, H., et al., 2002. Transmembrane collagen XVII, an epithelial adhesion protein, is shed from the cell surface by ADAMs. EMBO J. 21, 5026–5035.

Frederiks, W.M., Mook, O.R., 2004. Metabolic mapping of proteinase activity with emphasis on *in situ* zymography of gelatinases: review and protocols. J. Histochem. Cytochem. 52, 711–722.

Gawlak, M., Gorkiewicz, T., Gorlewicz, A., et al., 2009. High resolution *in situ* zymography reveals matrix metalloproteinase activity at glutamatergic synapses. Neuroscience 158, 167–176.

Henninger, N., Feldmann Jr., R.E., Futterer, C.D., et al., 2007. Spatial learning induces predominant downregulation of cytosolic proteins in the rat hippocampus. Genes Brain Behav. 6, 128–140.

Hernandez, A.I., Wolk, J., Hu, J.Y., et al., 2009. Poly-(ADP-ribose) polymerase-1 is necessary for long-term facilitation in Aplysia. J. Neurosci. 29, 9553–9562.

Hwang, J.J., Park, M.H., Choi, S.Y., et al., 2005. Activation of the Trk signaling pathway by extracellular zinc. Role of metalloproteinases. J. Biol. Chem. 280, 11995–12001.

Meighan, S.E., Meighan, P.C., Choudhury, P., et al., 2006. Effects of extracellular matrix-degrading proteases matrix metalloproteinases 3 and 9 on spatial learning and synaptic plasticity. J. Neurochem. 96, 1227–1241.

Meighan, P.C., Meighan, S.E., Davis, C.J., et al., 2007. Effects of matrix metalloproteinase inhibition on short- and long-term plasticity of schaffer collateral/CA1 synapses. J. Neurochem. 102, 2085–2096.

Michaluk, P., Kolodziej, L., Mioduszewska, B., et al., 2007. Beta-dystroglycan as a target for MMP-9, in response to enhanced neuronal activity. J. Biol. Chem. 282, 16036–16041.

Mizoguchi, H., Yamada, K., Mouri, A., et al., 2007. Role of matrix metalloproteinase and tissue inhibitor of MMP in methamphetamine-induced behavioral sensitization and reward: implications for dopamine receptor down-regulation and dopamine release. J. Neurochem. 102, 1548–1560.

Mungall, B.A., Pollitt, C.C., 2001. *In situ* zymography: topographical considerations. J. Biochem. Biophys. Methods 47, 169–176.

Murphy, G., Nagase, H., 2011. Localizing matrix metalloproteinase activities in the pericellular environment. FEBS J. 278, 2–15.

Nagy, V., Bozdagi, O., Matynia, A., et al., 2006. Matrix metalloproteinase-9 is required for hippocampal late-phase long-term potentiation and memory. J. Neurosci. 26, 1923–1934.

Nagy, V., Bozdagi, O., Huntley, G.W., 2007. The extracellular protease matrix metalloproteinase-9 is activated by inhibitory avoidance learning and required for long-term memory. Learn. Mem. 14, 655–664.

Nicoll, R.A., Schmitz, D., 2005. Synaptic plasticity at hippocampal mossy fibre synapses. Nat. Rev. Neurosci. 6, 863–876.

Odake, S., Morita, Y., Morikawa, T., et al., 1994. Inhibition of matrix metalloproteinases by peptidyl hydroxamic acids. Biochem. Biophys. Res. Commun. 199, 1442–1446.

Ogata, Y., Itoh, Y., Nagase, H., 1995. Steps involved in activation of the pro-matrix metalloproteinase 9 (progelatinase B)-tissue inhibitor of metalloproteinases-1 complex by 4-aminophenylmercuric acetate and proteinases. J. Biol. Chem. 270, 18506–18511.

Okulski, P., Jay, T.M., Jaworski, J., et al., 2007. TIMP-1 abolishes MMP-9-dependent long-lasting long-term potentiation in the prefrontal cortex. Biol. Psychiatry 62, 359–362.

Overall, C.M., 2002. Molecular determinants of metalloproteinase substrate specificity: matrix metalloproteinase substrate binding domains, modules, and exosites. Mol. Biotechnol. 22, 51–86.

Remmele, W., Stegner, H.E., 1987. Recommendation for uniform definition of an immunoreactive score (IRS) for immunohistochemical estrogen receptor detection (ER-ICA) in breast cancer tissue. Pathologe 8, 138–140.

Rivera, S., Khrestchatisky, M., Kaczmarek, L., et al., 2010. Metzincin proteases and their inhibitors: foes or friends in nervous system physiology? J. Neurosci. 30, 15337–15357.
Sang, Q.X., Birkedal-Hansen, H., Van Wart, H.E., 1995. Proteolytic and non-proteolytic activation of human neutrophil progelatinase B. Biochim. Biophys. Acta 1251, 99–108.
Spolidoro, M., Putignano, E., Munafo, C., et al., 2012. Inhibition of matrix metalloproteinases prevents the potentiation of nondeprived-eye responses after monocular deprivation in juvenile rats. Cereb. Cortex 22, 725–734.
Szklarczyk, A., Conant, K., 2010. Matrix metalloproteinases, synaptic injury, and multiple sclerosis. Front. Psychiatry 1, 130.
Szklarczyk, A., Lapinska, J., Rylski, M., et al., 2002. Matrix metalloproteinase-9 undergoes expression and activation during dendritic remodeling in adult hippocampus. J. Neurosci. 22, 920–930.
Szklarczyk, A., Oyler, G., McKay, R., et al., 2007. Cleavage of neuronal synaptosomal-associated protein of 25 kDa by exogenous matrix metalloproteinase-7. J. Neurochem. 102, 1256–1263.
Tian, L., Stefanidakis, M., Ning, L., et al., 2007. Activation of NMDA receptors promotes dendritic spine development through MMP-mediated ICAM-5 cleavage. J. Cell Biol. 178, 687–700.
Wang, X.B., Bozdagi, O., Nikitczuk, J.S., et al., 2008. Extracellular proteolysis by matrix metalloproteinase-9 drives dendritic spine enlargement and long-term potentiation coordinately. Proc. Natl. Acad. Sci. U. S. A. 105, 19520–19525.
Wang, H.H., Hsieh, H.L., Yang, C.M., 2011. Nitric oxide production by endothelin-1 enhances astrocytic migration via the tyrosine nitration of matrix metalloproteinase-9. J. Cell. Physiol. 226, 2244–2256.
Wlodarczyk, J., Mukhina, I., Kaczmarek, L., et al., 2011. Extracellular matrix molecules, their receptors and secreted proteases in synaptic plasticity. Dev. Neurobiol. 71, 1040–1053.
Wojtowicz, T., Mozrzymas, J.W., 2010. Late phase of long-term potentiation in the mossy fiber-CA3 hippocampal pathway is critically dependent on metalloproteinases activity. Hippocampus 20, 917–921.
Wright, J.W., Masino, A.J., Reichert, J.R., et al., 2003. Ethanol-induced impairment of spatial memory and brain matrix metalloproteinases. Brain Res. 963, 252–261.
Wright, J.W., Meighan, S.E., Murphy, E.S., et al., 2006. Habituation of the head-shake response induces changes in brain matrix metalloproteinases-3 (MMP-3) and −9. Behav. Brain Res. 174, 78–85.
Yang, Y., Candelario-Jalil, E., Thompson, J.F., et al., 2010. Increased intranuclear matrix metalloproteinase activity in neurons interferes with oxidative DNA repair in focal cerebral ischemia. J. Neurochem. 112, 134–149.
Yong, V.W., 2005. Metalloproteinases: mediators of pathology and regeneration in the CNS. Nat. Rev. Neurosci. 6, 931–944.
Zhang, J.W., Gottschall, P.E., 1997. Zymographic measurement of gelatinase activity in brain tissue after detergent extraction and affinity-support purification. J. Neurosci. Methods 76, 15–20.